Master's Thesis

Experimental Study on Plasmofluidic Disk Resonators Filled with Liquid Crystal

Quoc Viet Vuong

Department of Electrical Engineering

Graduate School of UNIST

2018

Experimental Study on Plasmofluidic Disk Resonators Filled with Liquid Crystal

Quoc Viet Vuong

Department of Electrical Engineering

Graduate School of UNIST

Experimental Study on Plasmofluidic Disk Resonators Filled with Liquid Crystal

A thesis
submitted to the Graduate School of UNIST
in partial fulfillment of the
requirements for the degree of
Master of Science

Quoc Viet Vuong

06/14/2018 of submission
Approved by

Advisor
Min-Suk Kwon

Experimental Study on Plasmofluidic Disk Resonators Filled with Liquid Crystal

Quoc Viet Vuong

This certifies that the thesis of Quoc Viet Vuong is approved.

06/14/2018 of submission

signature

Advisor: Min-Suk Kwon

signature

Il-Sug Chung: Thesis Committee Member #1

signature

Jongwon Lee: Thesis Committee Member #2

TABLE OF CONTENTS

LIST OF FIGURES

Nomenclature

PDRs	Plasmofluidic disk resonators
CMOS	Complementary metal-oxide-semiconductor
MISIM	Metal-Insulator-Semiconductor-Insulator-Metal
HPWs	Hybrid plasmonic waveguides
LC	Liquid crystal
TLS	Tunable laser source
PC	Polarization controller
SMF	Single-mode fiber
LF	Lens fiber
PH	Peltier heater
TC	Thermalcoupler

Abstract

Optical resonators have been widely used due to its wavelength-selective characteristics. When light is launched into the bus waveguide of a resonator, the resonance wavelength can be determined via its resonance spectrum. For this advantage, optical resonators have been especially utilized for sensing application and tuning. In this research, the novel waveguide and resonator structure, which is Plasmofluidic Disk Resonators (PDRs) coupled to Metal-insulator-semiconductor-insulator-metal (MISIM) waveguide is briefly introduced. Then, this fabricated structure, combined with liquid crystal controlled by temperature to tune the resonance characteristics, has been simulated and experimentally studied. The simulation result shows that when the temperature rises from the lowest (26°C) to the highest (65°C), the wavelength shift is about 30-nm blue shift. The experimental result shows the corresponding wavelength shift is about 10-nm blue shift. With this result, it is expected that the liquid crystal can be controlled by electric field for this structure, open a research direction for a novel form of modulator.

1. Introduction

1.1. Silicon photonics

Silicon photonics has been one of the solutions and platforms for high-scale integrated optics for decades. It enables design on a larger scale and shifting from component-oriented design to circuit-oriented design. Silicon photonics helps integrate many optical functions on a chip using the fabrication technology of CMOS industry, thereby facilitates low cost, large volume manufacturing. A growing number of manufacturing and prototyping facilities have enabled silicon photonics to become an industrial platform [1]. There are two main factors that contribute to the viability of silicon photonics: high refractive index contrast and CMOS compatibility. High refractive index contrast between silicon and silicon dioxide enables designed size of the optical waveguide, which is a key component for photonic integrated circuits, to be of sub-micrometer dimensions, which in turn, allows for dense packaging on a chip [1]. Thanks to CMOS compatibility, manufacturing cost has been substantially reduced and high-volume manufacturing has been enabled. Fabrication process for silicon photonics have become good enough to make large, complex circuits, with waveguide losses smaller than 1 dB/cm, low-loss crossings [12], splitters [7-11], couplers [13] as well as good modulators [8] and excellent photodetectors [15].

However, high refractive index contrast also has low fabrication tolerance, i.e., the overall performance of a photonic circuit will endure a significant impact just because of a seemingly non-negligible nanometer-scale variation [1]. Often, a photonic circuit performance is usually affected by light scattering from sidewall roughness, which is unavoidable and considered to be the strongest effect. Therefore, many attempts have been exerted to minimize this roughness [4].

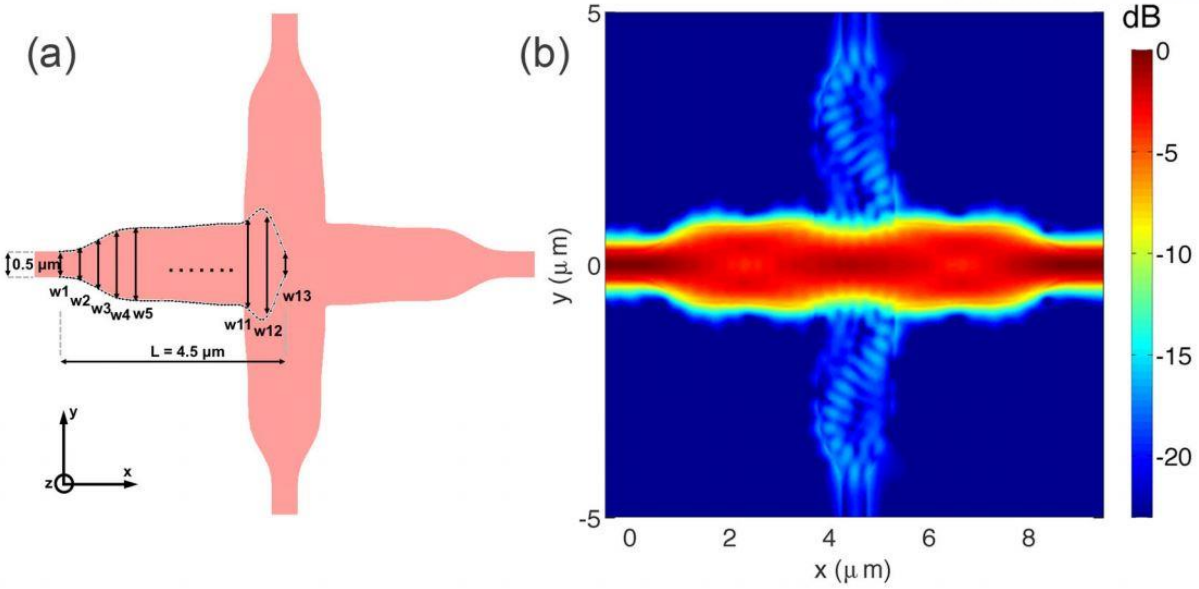

Figure 1-1: Example of a silicon photonic crossing [12].

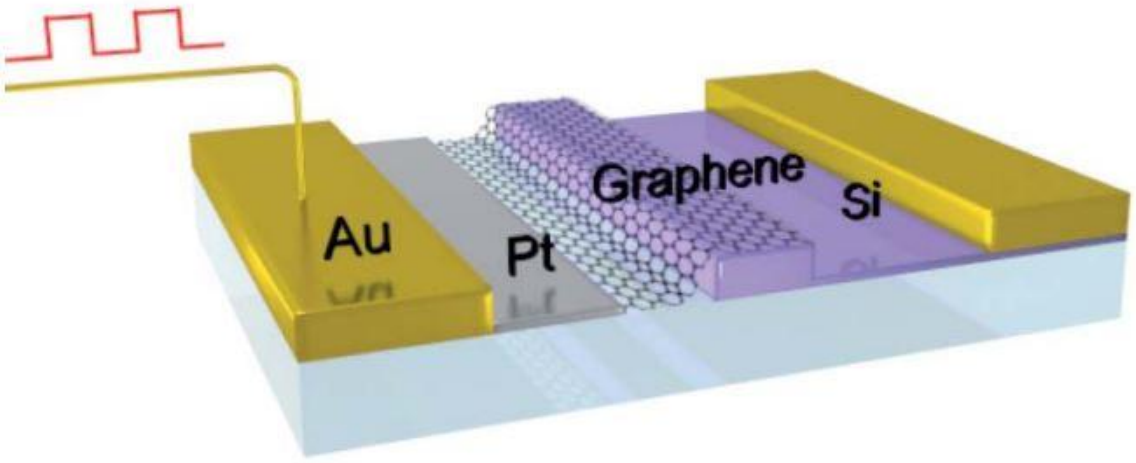

Figure 1-2: Example of a silicon photonic modulator [8].

Another weakness of conventional silicon photonics waveguides and devices, which are mainly based on the high refractive contrast between silicon and silicon dioxide is the limitation on mode size and device size. Due to the diffraction limit, the mode size miniaturization is challenging. The size of, for example, a ring resonator, is also limited by the function of its design target. Therefore, it is also challenging to miniaturize the devices in conventional silicon photonic circuits.

To overcome these drawbacks, many unconventional silicon photonic devices, which operate using

surface plasmon polaritons, have been studied and developed. For plasmonic waveguide, using plasmon polariton, the diffraction limit can be overcome, reducing the size of the mode to tens of nanometers. The hybrid plasmonic waveguides (HPWs), which utilize the low propagation loss of dielectric waveguides, and the sub-wavelength mode confinement of the plasmonic waveguides, have been a great solution for silicon photonic circuits.

In this thesis, the unconventional hybrid plasmonic device, namely metal-insulator-semiconductor-insulator-metal (MISIM) plasmofluidic disk resonators (PDRs), which consists of a MISIM waveguide coupled with a silicon disk resonator surrounded by copper with a 30-nm channel in between, has been studied and analyzed experimentally. The channel was initially silicon dioxide, so wet-etching was used for removing the oxide, forming a channel that can be filled with liquid material. Refractive index oils and liquid crystals were used to fill the channel; and the resonance characteristics of the PDRs were analyzed in each case. In the case of liquid crystals, the resonance spectrum was measured at various temperature to investigate the variability of resonance characteristics of the PDRs when the refractive indices of the liquid crystal were controlled by temperature. It is expected in the future that the resonance wavelength can be tuned by controlling the liquid crystal's refractive indices by electric field instead of temperature, paving the way for a prospect of electro-optic modulator.

1.2. Optical Resonators based on Silicon Photonics

Optical resonator has been a familiar photonic device which has applications such as optical signal processing and sensing, based on wavelength-selective characteristics. The basic function of the optical resonator is to store light at a specific wavelength, making optical resonators one of the wavelength-selective devices. Optical resonators have a wide range of applications including resonator-based sensors. Those optical resonator-based sensors, some of which are in the form of microring or microdisk, operate by sensing refractive index change in the waveguide cladding. The variation of the refractive index leads to the change in the modal effective index, which results in a wavelength shift. The more the evanescent field infiltrate into the cladding, the longer phase shift the resonators will produce. The following resonance equation shows the relation between the modal effective index and the resonance wavelength:

$$\lambda_{res} = \frac{2\pi R n_{eff}}{m}$$

Where λ denotes the wavelength, m being the integer mode order, and R being the disk radius. From

the equation we can see that the resonators support multiple resonances, the spacing between the resonance dips is call free spectral range (FSR). To target higher FSR, the size of the ring or disk must be reduced, causing challenge for the silicon photonic technology: the small bending radius must be achieved. Also, it poses a requirement for high-contrast waveguides with strong confinement, to restrict the bending loss.

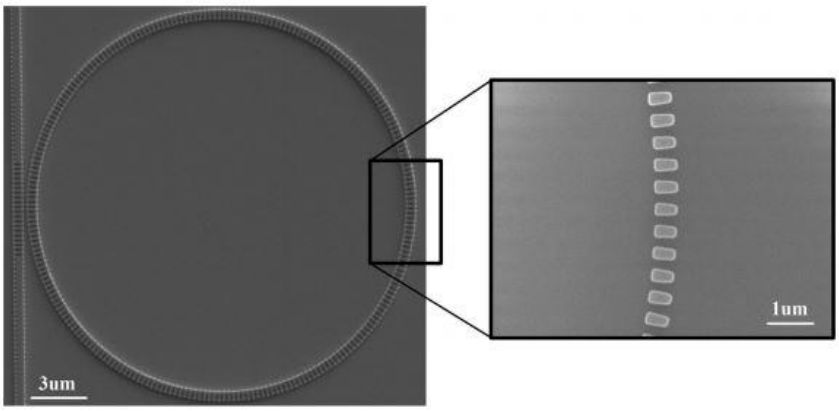

Figure 1-3: Reported silicon photonic based microring resonator [9].

1.3. Hybrid Plasmonic Waveguides (HPWs)

The conventional dielectric waveguides, which are based on total internal reflection for light guiding, can guide light over a long distance with low loss. However, the mode size is limited by the diffraction. Plasmonic waveguides, on the other hand, utilize surface plasmon to confine light near a metal surface. The mode in plasmonic waveguides is not limited by diffraction, thus can be confined in a very small volume. However, plasmonic waveguides suffer large propagation loss due to light dissipation in the metal. Therefore, the design of the hybrid plasmonic waveguides (HPWs) attempts to combine the two merits of both waveguides. The typical design of the HPWs consists of a silicon nanowire placed very close to a metal surface and separated by a very thin layer of insulator. The silicon nanowire supports the dielectric waveguide mode, which is confined inside silicon. The metal layer supports surface plasmonic mode, which is confined near the metal surface. These two modes, when brought close together appropriately, will couple to each other, yielding the hybrid plasmonic mode, which has both low propagation loss and small mode volume. The small volume of the mode can be achieved due to the confinement of the electric field inside the thin insulator layer (or layers), whose refractive index is low.

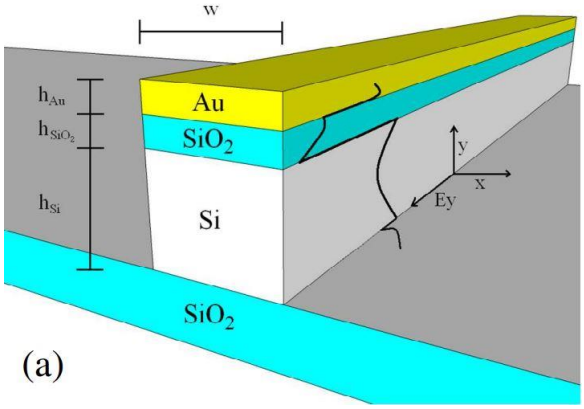

Figure 1-4: One of the reported MIS hybrid plasmonic waveguide [16].

There have been various hybrid plasmonic waveguides reported recently, many of which are metal-insulator-semiconductor (MIS) waveguides, which consist of rectangular layers of metal, insulator (mostly silicon dioxide) and semiconductor (mostly silicon) vertically stacked upon one another. The hybrid plasmonic waveguide with a gold layer deposited onto silicon, separated by a thin layer of silicon dioxide, has been reported in Figure 1-4. The waveguide has a subwavelength confinement inside the silicon dioxide layer with a good propagation length of 40μm [16].

However, the vertically stacked MIS waveguide structure mentioned above has some drawbacks. First, the vertically stacked structures are prone to alignment errors, which can deviate the realized structure from the ideally designed structure [6]. Second, tuning the mode is challenging. The silicon wire's refractive index may be adjusted using carrier injection or depletion method, but it requires p-i-n structure, and the response speed is not very high. It would be more effective to tune the refractive index of the insulator layer instead, but it is not easy to adjust the refractive index of silicon dioxide. Even worse, the insulator layer cannot be replaced by any functional material due to being covered by another layer upon it [6]. The Metal-Insulator-Silicon-Insulator-Metal (MISIM) waveguide, which is introduced in the following section overcome the two above mentioned drawbacks of the MIS structure.

1.4. Metal-Insulator-Silicon-Insulator-Metal (MISIM) waveguides

The metal-insulator-silicon-insulator-metal (MISIM) waveguide is a different type of hybrid plasmonic waveguides. The layers are not vertically stacked but horizontally placed next to one another. The oxide layer was deposited upon silicon waveguide pattern, and then the metal layer (copper in this case) was

deposited upon oxide layer, together creating the metal-insulator-silicon-insulator-metal placing side-by-side horizontally, as shown in Figure 1-5. The horizontal placement of layers allows the U-shaped silicon dioxide layer to be removed by wet-etching and replaced by other functional material such as electro-optic materials or liquid crystal. The schematic view of the etched waveguide is depicted in Figure 1-6.

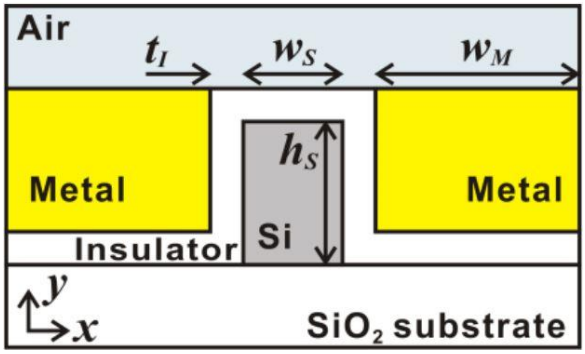

Figure 1-5: MISIM waveguide structure with un-etched silicon dioxide insulator channel [6].

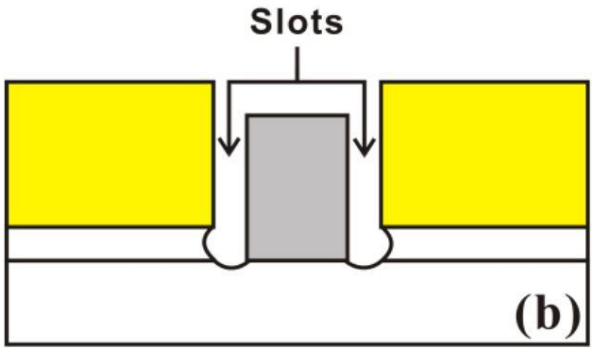

Figure 1-6: MISIM waveguide structure with silicon dioxide insulator removal [6].

According to the simulation results, as shown in Figure 1-7, most of the light power carried by the waveguide is confined in the two thin insulator layers. The confinement of the mode inside the silicon dioxide layers proves that the hybrid plasmonic mode supported by the MISIM waveguide has a very small size.

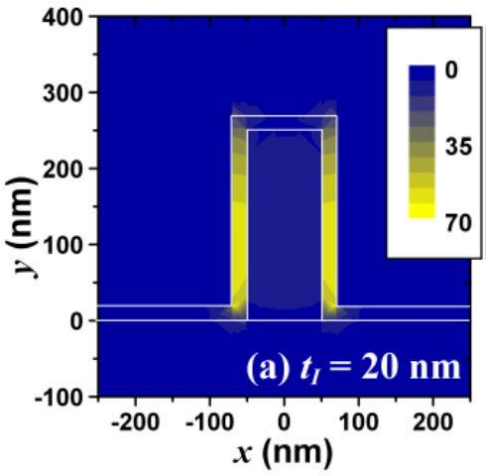

Figure 1-7: The simulation result for the mode shape of MISIM waveguide [6].

1.5. Plasmofluidic Disk Resonators (PDRs) based on MISIM waveguides

The plasmofluidic disk resonators (PDRs) are the resonators with disk structure coupled with MISIM waveguides. A PDR consists of a sub-micrometer radius silicon disk and metal surrounding the disk with 30-nm channel in between. The channel, after wet-etching, can be filled with fluid, and the resonance mode is confined in the fluid. When light propagates inside the waveguide, at a certain wavelength, the light will be coupled to the disk, causing energy storage inside the disk, which is called resonance. Because of the wavelength-selective light energy storing characteristics, the PDRs have a propitious application as sensors. The disk is designed and fabricated along with the MISIM waveguide as shown in Figure 1-8 and Figure 1-9. The channel width is 30-nm, like the width of silicon dioxide layer in MISIM waveguides.

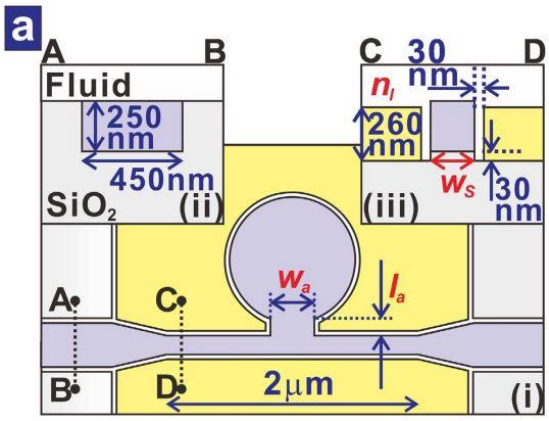

Figure 1-8: Schematic view of a PDR coupled with a MISIM waveguide [17].

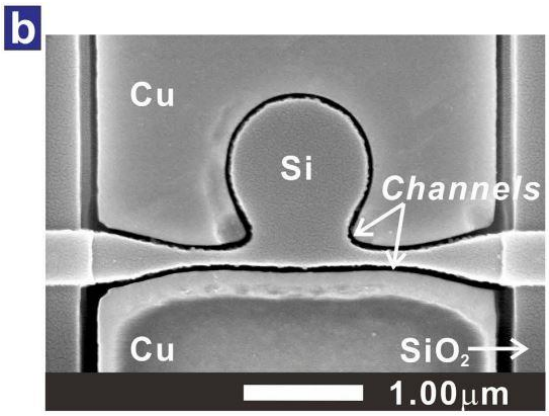

Figure 1-9: SEM image of a fabricated PDR coupled with MISIM waveguide [17].

The advantage of the PDRs over silicon photonic resonators is that the effective volume of the PDRs is reduced, thus reducing the footprint. The electric field of the mode is confined in a narrow, low-refractive-index region silicon dioxide layer between metal and silicon. Moreover, the designed MISIM structure is compatible with standard complementary metal-oxide-semiconductor (CMOS) technology, thus enabling easy integration with other silicon photonic devices.

1.6. Thesis approach: PDRs for liquid crystal application

In this research, the PDRs are combined with liquid crystals, which is poured directly onto the sample surface and supposedly fills the resonator's channel. Liquid crystal is a well-known birefringence material whose refractive indices vary under temperature or electric field. By controlling the refractive indices of the liquid crystal, by means of temperature or electric field, the resonance characteristics of the PDRs can be tuned, leading to a potential opportunity for opto-electrical modulator.

Within the limit of this thesis, the liquid crystal's refractive indices are controlled by means of temperature only. It is easier to implement and it is also meaningful to investigate the impact of temperature on the operation of PDRs with liquid crystals. To investigate the operation with electric field, however, more sophisticated fabrication steps need to be done.

2. Theoretical investigation

When the liquid crystal fills the channel, the positional and orientational order of the LC molecules inside the channel play a basic role in determining the resonance characteristics of the PDRs. Therefore, some theory about birefringence, positional and orientational order of LC molecules inside the channel needs to be reviewed.

2.1. Liquid Crystal (LC) – filled PDRs based on MISIM waveguides

In this thesis, the liquid crystal (LC) E7 was used for both theoretical simulation and experimentally applied on the PDRs. The E7 LC molecules are rod-like (calamitic) molecules, i.e., the molecular structure of each LC molecule has a shape of a long rod. The molecules possess not only positional order but also orientational order. This is because liquid crystals are mesophases between isotropic liquid and crystalline solid [18].

At very high temperature, the liquid crystal exhibits isotropic characteristics, in which the LC molecules have neither positional nor orientational order [18]. When the temperature is lowered, the LC turns into the most common phase, namely nematic. In the nematic phase, due to the orientational order, the long axis of the rod-like LC molecules have a preferred direction, the average of which is called liquid crystal director [18], and denoted as $\vec{n}$, as illustrated in Figure 2-1.

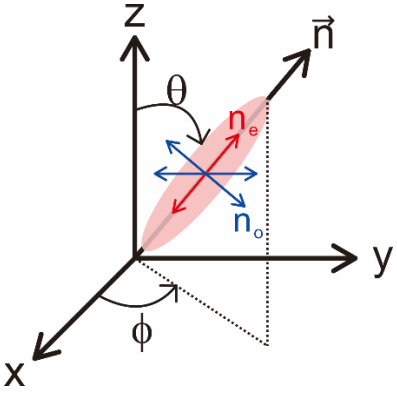

Figure 2-1: Schematic view of a rod-like liquid crystal molecule, which has the ordinary index (n_o) with respect to the short axis and the extra ordinary index (n_e) with respect to the long axis.

Regarding optical characteristics, the liquid crystals are birefringence materials, which have the ordinary refractive index (n_o) along the direction of the short axis and the extraordinary refractive index

(n_e) along the direction of the long axis. When these molecules gather to form liquid crystals, the n_o and n_e are broader terms which indicate the ordinary index and extraordinary index of the whole material in general. Therefore, when the temperature varies, the positional and orientational order of the LC molecules change accordingly, which lead to the change in n_o and n_e themselves, which is indicated in Figure 2-2 and Figure 2-3.

λ (μm)					
	1.55			10.6	
T (°C)	n_e	n_o	T (°C)	n_e	n_o
15.6	1.70869	1.50928	18.6	1.69624	1.49188
20.3	1.70004	1.51061	20.2	1.69271	1.494
26	1.69239	1.50895	26	1.68795	1.49294
29.1	1.68706	1.50661	29.6	1.68459	1.49964
35.2	1.67841	1.50495	36.2	1.67454	1.49417
40.4	1.66976	1.50562	40.7	1.6726	1.49682
45.4	1.65744	1.50695	46.1	1.66271	1.49929
49.6	1.65145	1.50761	50.1	1.66042	1.49805
55.5	1.62782	1.51427	55	1.65389	1.50088
58.6	1.60551	1.51827	57	1.62777	1.50829
60.6	1.54858	1.54858	57.2	1.61154	1.51447
65	1.54558	1.54558	57.4	1.60271	1.51447
68.5	1.54425	1.54425	57.8	1.59989	1.51729

Figure 2-2: Measured refractive indices (n_e and n_o) of the liquid crystal E7 at the wavelength 1.55 μm and 10.6μm, at different temperatures [20].

As the temperature of the LC reaches or goes beyond a certain critical temperature, called “clearing temperature”, the LC becomes isotropic liquid, in which the ordinary index becomes equal to the extraordinary index [20]. As referring to Figure 2-2, at the temperature of 60.6 °C, $n_e = n_0 = 1.54858$. The clearing temperature of the LC E7 is around 58 °C [19].

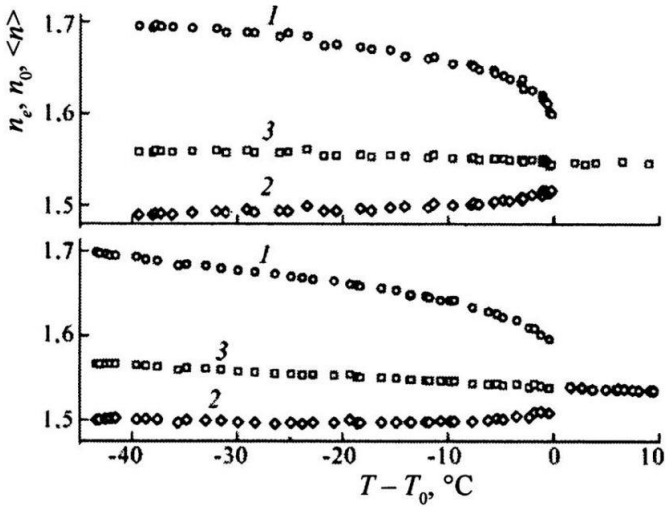

Figure 2-3: Values of n_e (1), n_o (2), and $\langle n \rangle = (2n_o + n_e)/3$ (3) for the nematic LC E7 as a function of temperature shift $T - T_0$, with T_0 being the clearing temperature. The upper graph and the lower graph show the values corresponding to the wavelength 1.55μm and 10.6μm, respectively.

2.2. Finite-difference time domain (FDTD) simulation for LC-filled PDRs

The Lumerical FDTD solution – a commercial finite-difference time domain (FDTD) program was used to simulate operation of the LC-filled PDRs. By FDTD, we tried to simulate theoretically the impact of varying temperatures on the operation of the PDRs whose channels are filled with LC. The simulated model of the PDRs is depicted in Figure 2-4.

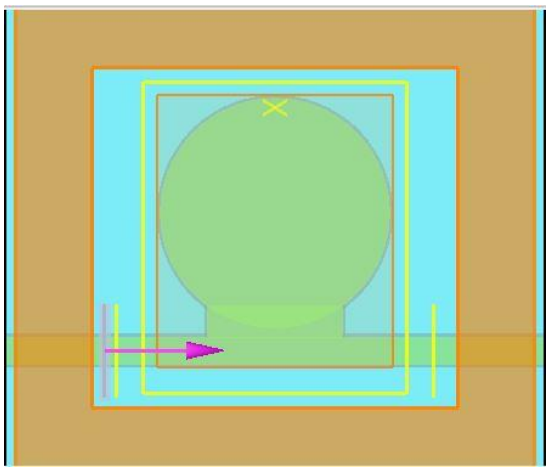

Figure 2-4: The simulation model for the PDRs whose channels are filled with LC.

To perform simulation, we modeled the LC-filled PDRs using the surface anchoring characteristics of LC molecules. The inner sidewall is silicon and the outer sidewall is copper. For copper, it was theoretically and experimentally observed that the LC molecules align perpendicular to the surface (homeotropic induced anchoring) [21]. For silicon, however, it is observed that the LC molecules align parallel with a preferred direction, i.e., the LC molecules have a planar uniform alignment (homogeneous anchoring) on the surface of silicon [23]. Therefore, we modelled the channel as depicted in Figure 2-5.

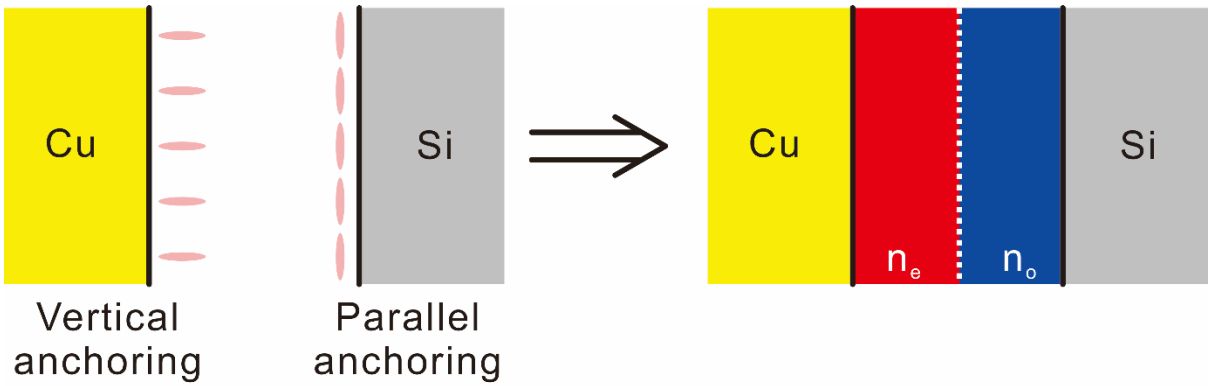

Figure 2-5: The modelling of the liquid crystal channels of the PDRs.

In our simulation, we divided the channel into two parts, as shown in Figure 2-5. The refractive index of the part close to the copper surface was assigned with extraordinary index n_e of the liquid crystal and the other part, which is adjacent to the silicon surface, was assigned with the ordinary index n_o of the liquid crystal. By performing several simulations and comparing the results, the appropriate ratio between the n_e region and the n_o region was decided to be 1:4. These indices' values change according to the change of temperature and were taken from Figure 2-2.

2.3. Simulation result of the PDRs filled with LC at different temperature

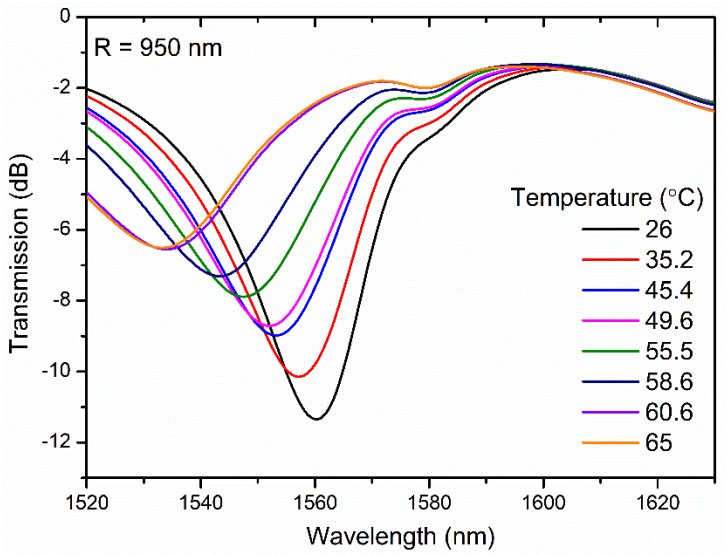

Figure 2-6: The simulated transmission spectrum for the PDR whose radius equals to 950 nm with various temperatures

Figure 2-6 shows the simulated transmission spectrum for the PDR whose radius equals to 950 nm. The simulation was performed with various temperature settings. As can be seen in Figure 2-6, as temperature increases, there is a blue-shift occurring to the resonance spectrum. Moreover, there is a sharp decline in the resonance wavelength as the temperature changes from 58.6 °C to 60.6 °C.

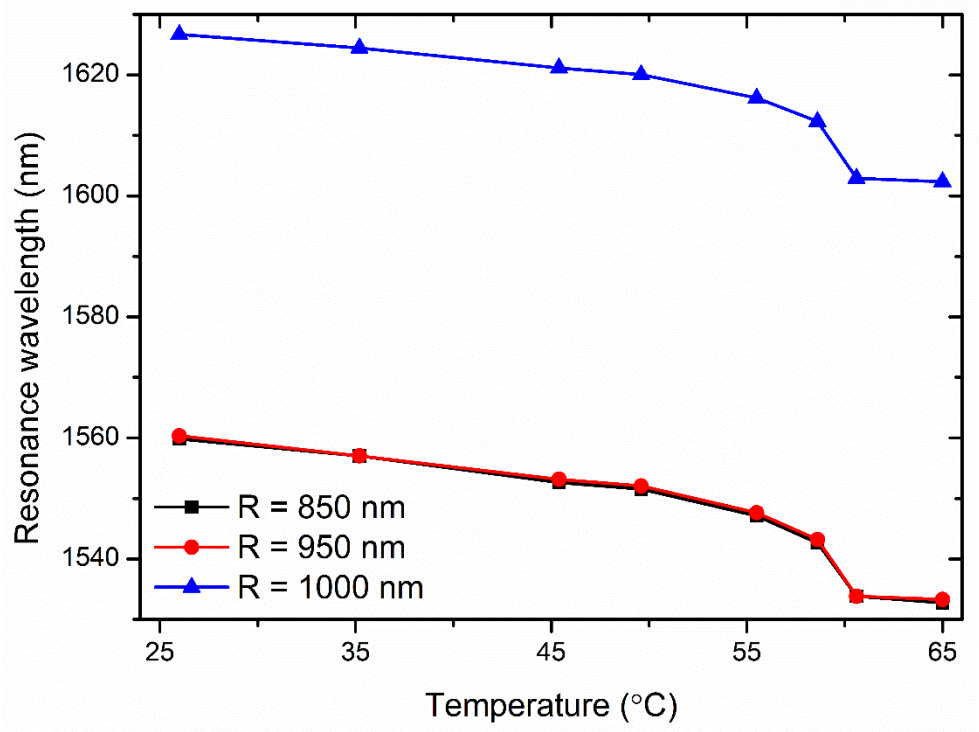

Figure 2-7: The simulated spectra with different temperatures of the LC-filled PDRs for different disk radii of 850, 950, and 1000 nm

The results of the simulation for different disk radii of 850 nm, 950 nm, 1000 nm with various temperatures were summarized in Figure 2-7. The resonance spectra of the PDRs with different radii blue-shifted as the temperature increases. This result can be explained as the following. At the low temperature, n_e is large, n_o is small so there is a big gap between n_e and n_o, which leads to the mode being confined more in the n_e region. When the temperature increases, however, n_e declines and n_o increases (see Figure 2-3), i.e., n_e and n_o move closer to each other. Therefore, the mode is more loosely confined in the channel, which leads to the drop of the effective index of the mode in the channel. The drop of the effective index leads to the decrease in resonance wavelength. Therefore, the resonance spectrum blue-shifts.

3. Experiments and Analysis

3.1. Experiments and Analysis method for LC-filled PDRs based on MISIM waveguides

The PDRs were fabricated on a chip by a commercial foundry. The chip was covered with a SU-8 2015 layer and a SU-8 microfluidic channel was made using photolithography. The sample was then dipped into BOE 6:1 solution in 30 seconds for removing the insulator (silicon dioxide) layer. Finally, the sample is washed thoroughly with DI water.

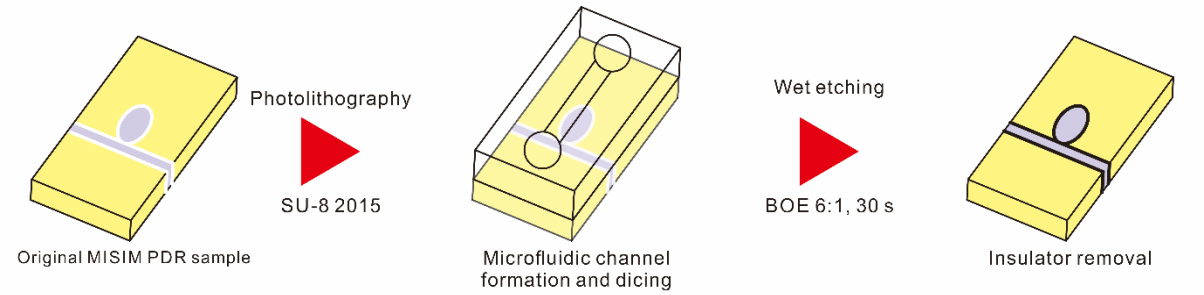

Figure 3-1: The fabrication flow of the making of SU-8 2015 microfluidic channel and insulator removal

For the setup of measurement system used for measuring the resonance characteristics of the PDRs, a tunable laser source (TLS) with light spectrum ranging from 1520 nm to 1630 nm was used. The laser source is connected to a polarization controller (PC) via a single-mode fiber (SMF), so that the quasi-TE mode is selected. The connection is then reduced from single-mode fiber to the lens fiber (LF). The tip of the lens fiber is placed in a very close proximity to the facet of the chip. On the other side of the chip, the lens fiber connects the chip to the photodiode (PD) via a single mode fiber to receive the transmission signal. The temperature of the chip is controlled using a Peltier heater, which is place under a metal stage. The chip is placed upon the stage with the thermal grease pasted underneath to increase thermal conductivity. The metal stage is connected to a thermometer for observing the temperature.

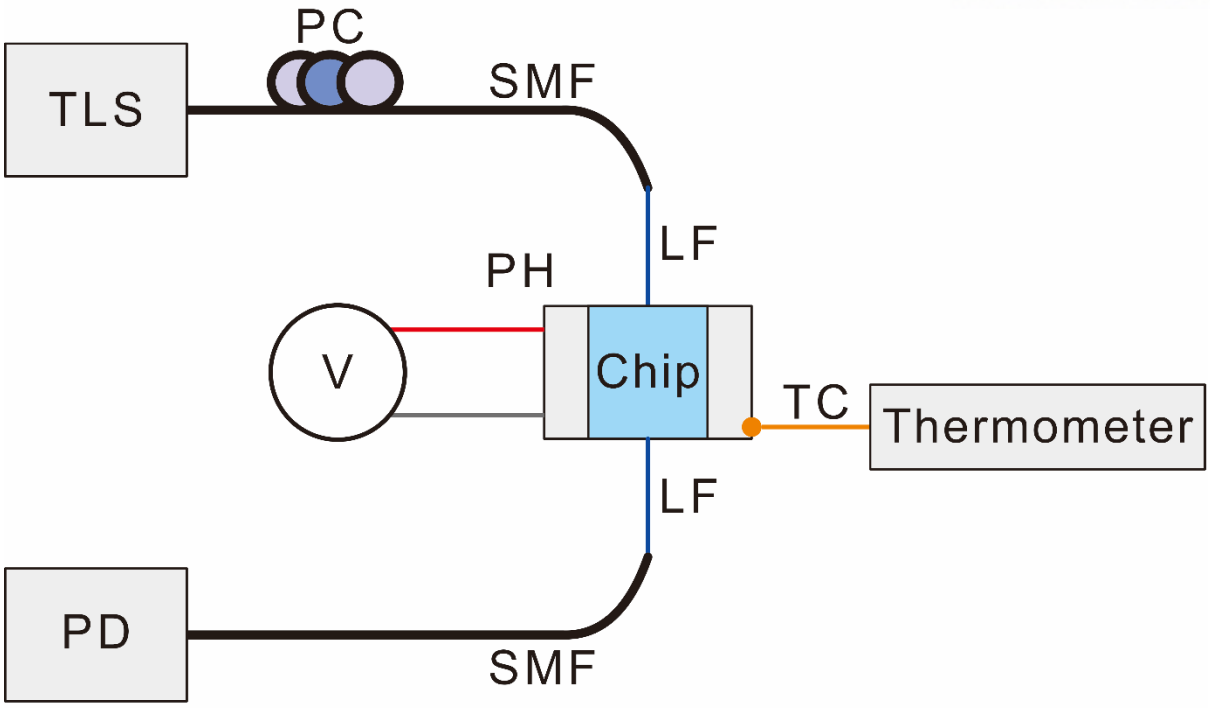

Figure 3-2: The setup of the measurement system used for measuring resonance characteristics of the PDRs

Regarding the experimental measurement, there are 3 samples of reference waveguide, which is identical to the one for coupling with the disk resonators. The insertion loss of the reference waveguide is taken as the average of the 3 samples. For each radius of the disk resonators, there are also 3 samples. When measuring, The TLS emits the light whose wavelengths are 1520 nm, 1521 nm…, with 1-nm step, one by one until the wavelength is 1530 nm. Each measurement took about 2 minutes. For the thermal controlling, after each measurement, the voltage was adjusted and it was waited for about 2 minutes for the temperature to become stable. Then a new measurement was started. The transmission spectrum of each radius is obtained by averaging the spectrum of 3 corresponding samples.

For data analyzation, there are 3 steps that need to be done. The first one is to "smooth" the transmission spectrum of both reference waveguides and the disk resonators. The second one is to normalize the transmission spectrum of the disk resonators, and the third one is to extract the resonance wavelength from the normalized spectrum of the disks.

The original transmission spectra of the PDRs contain lots of noise in the form of ripples, due to Fabry-Perot resonance of the chip. Therefore, they need to be smoothed. For this purpose, the adjacent averaging method was employed. The details of this method can be found at the supplementary information in [17]. To obtain normalized transmission spectrum, the principle is to subtract the

insertion loss of the reference waveguides from the transmission spectra of the PDRs.

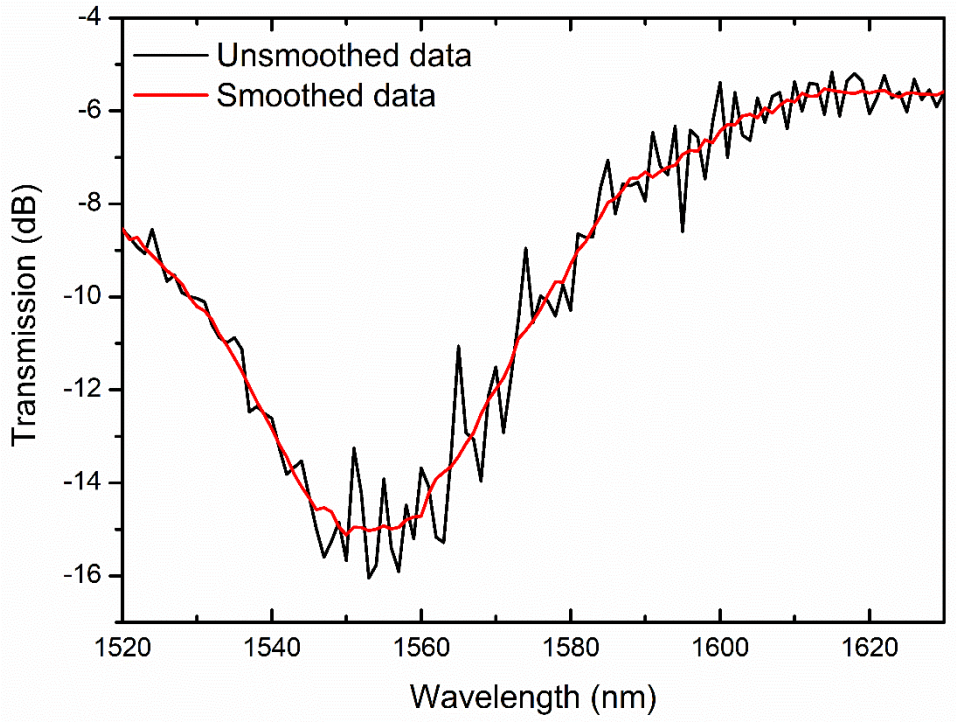

Figure 3-3: The raw and smoothed example transmission spectrum of a PDR correspond to the radius of 950 nm

The last step to be done is to extract the resonance wavelength from the transmission spectra. To do so, the centroid algorithm was used. Details of this algorithm can be found in [25].

3.2. Experimental Results

The PDRs experiments were conducted in 2 cases: with refractive index oils and with liquid crystal. In the case of liquid crystal, the experiments were conducted with various temperatures.

3.2.1. Case 1: Experimental results of PDRs filled with various refractive-index oils

The purpose of the experiments with refractive index oils is to check the wavelength shift of the resonance spectra when the refractive index is changed. Two kinds of oil which was employed had the refractive indices of 1.44 and 1.53. After pouring one kind of oil, the chip was washed thoroughly by methanol, dried and then poured another oil at the next time.

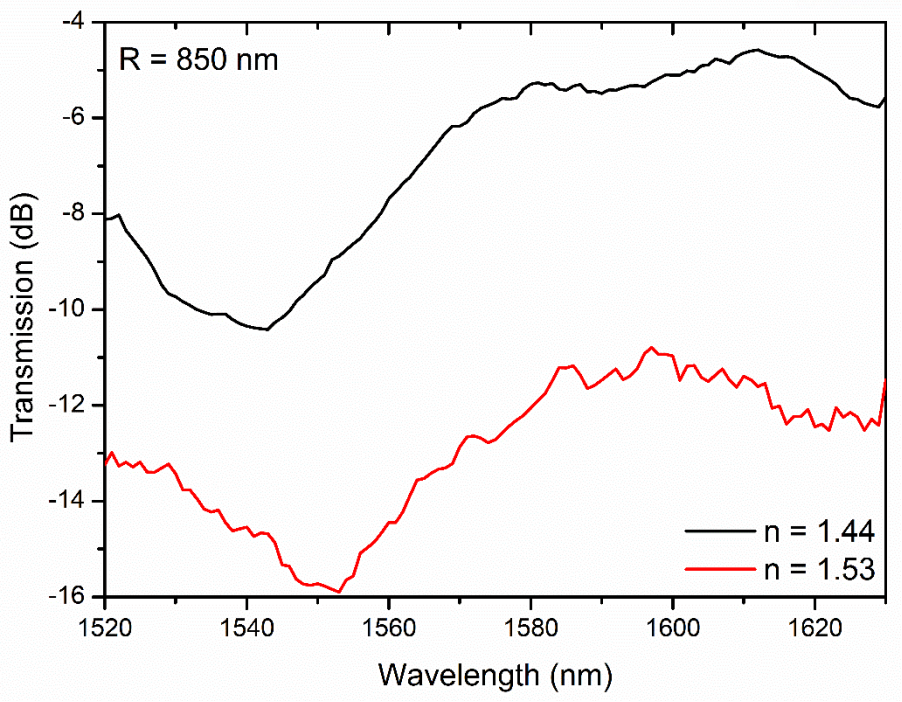

Figure 3-4: Transmission spectra of the PDRs with radius of 850 nm for refractive index oils of 1.44 and 1.53

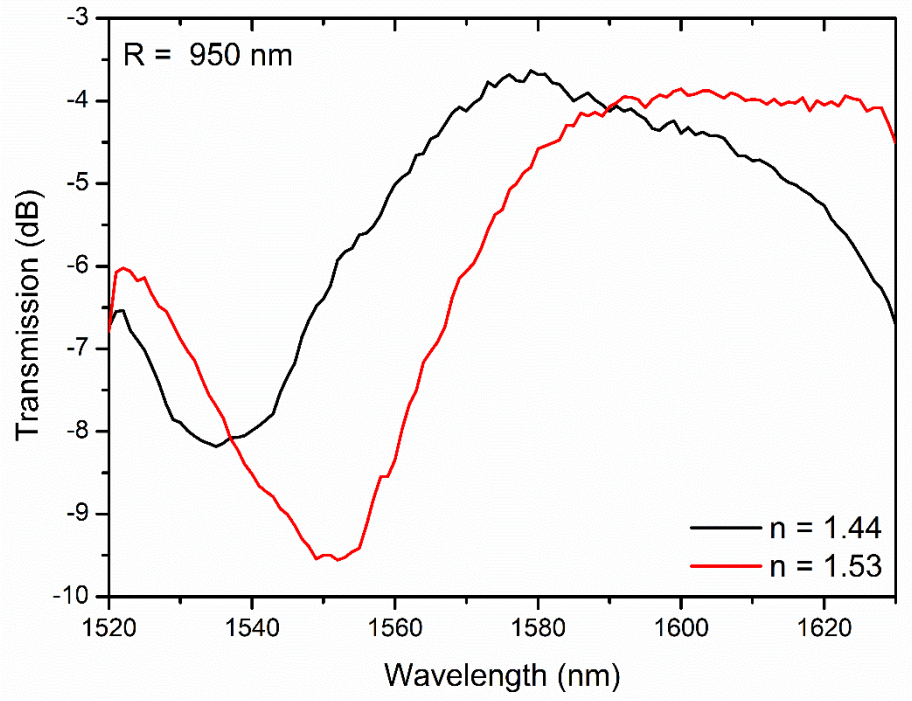

Figure 3-5: Transmission spectra of the PDRs with radius of 950 nm for the refractive index oils of 1.44 and 1.53

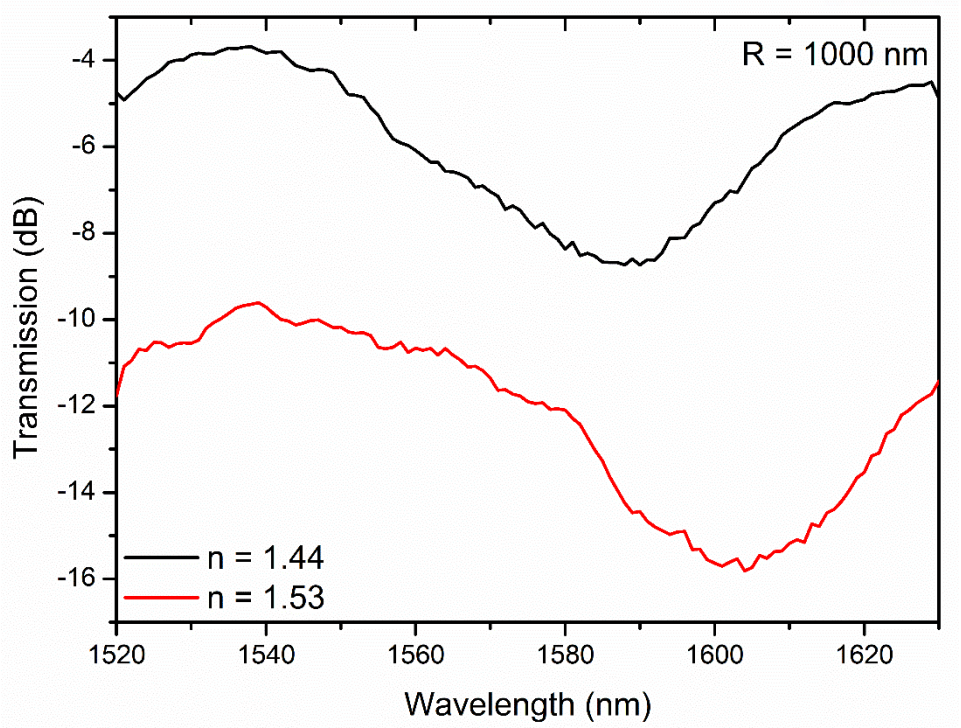

Figure 3-6: Transmission spectra of the PDRs with radius of 1000 nm for refractive index oils of 1.44 and 1.53

The measured transmission spectra of the PDRs with different radii of 850 nm, 950 nm, and 1000 nm are given in Figure 3-4, Figure 3-5 and Figure 3-6. A spectra red-shift of 10-15 nm was observed for every radius of the PDRs as the refractive index oil was increased from 1.44 and 1.53.

3.2.2. Case 2: Experimental results of LC-filled PDRs with temperature control

This is the main experiment in this research. The experiment of LC-filled PDRs with various temperatures is aimed to compare the experimental wavelength shift of the resonance spectra with the simulated wavelength shift. The dependence of resonance wavelength on temperature is shown in Figure 3-7, Figure 3-8 and Figure 3-9.

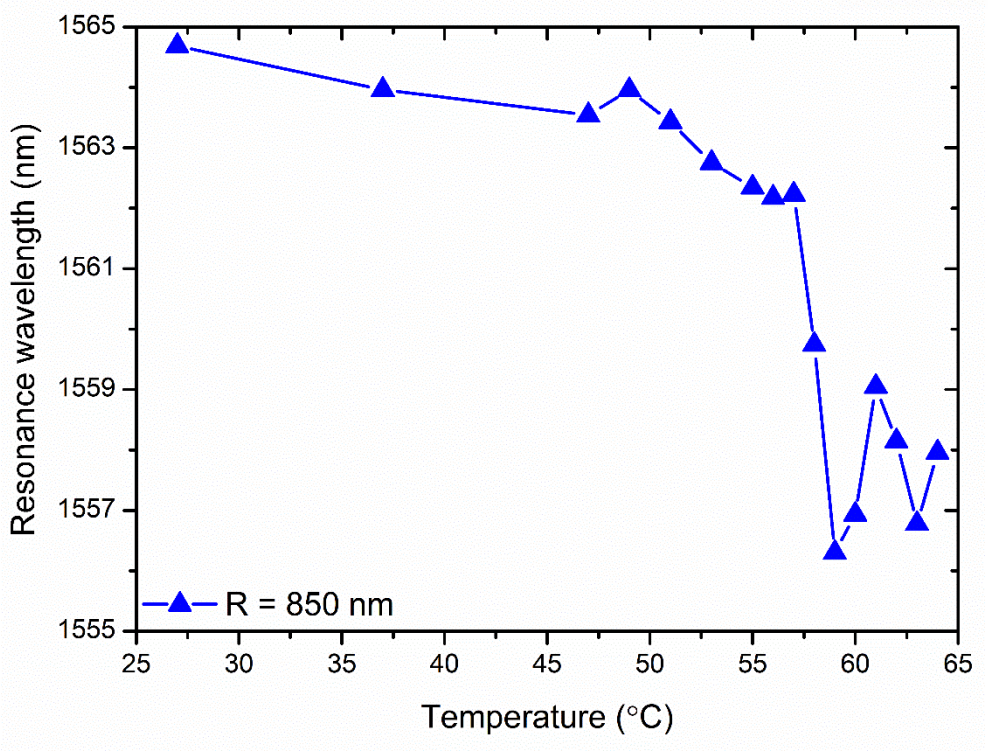

Figure 3-7: Temperature dependence of resonance wavelength in the experiment with LC E7 for the disk radius of 850 nm

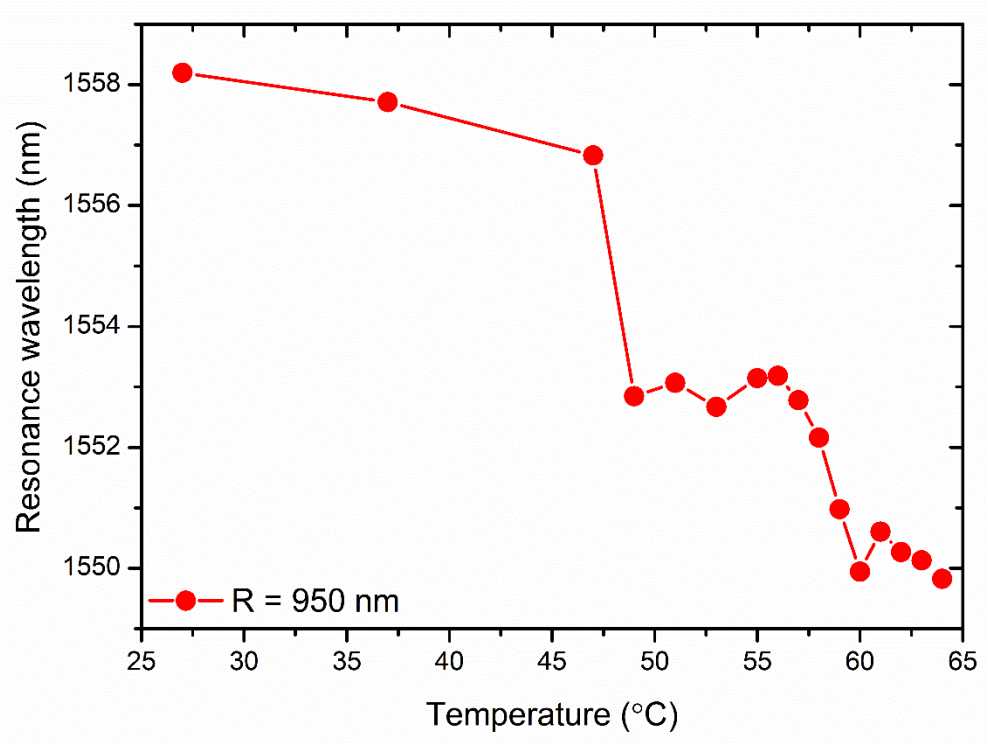

Figure 3-8: Temperature dependence of resonance wavelength in the experiment with LC E7 for the disk radius of 950 nm

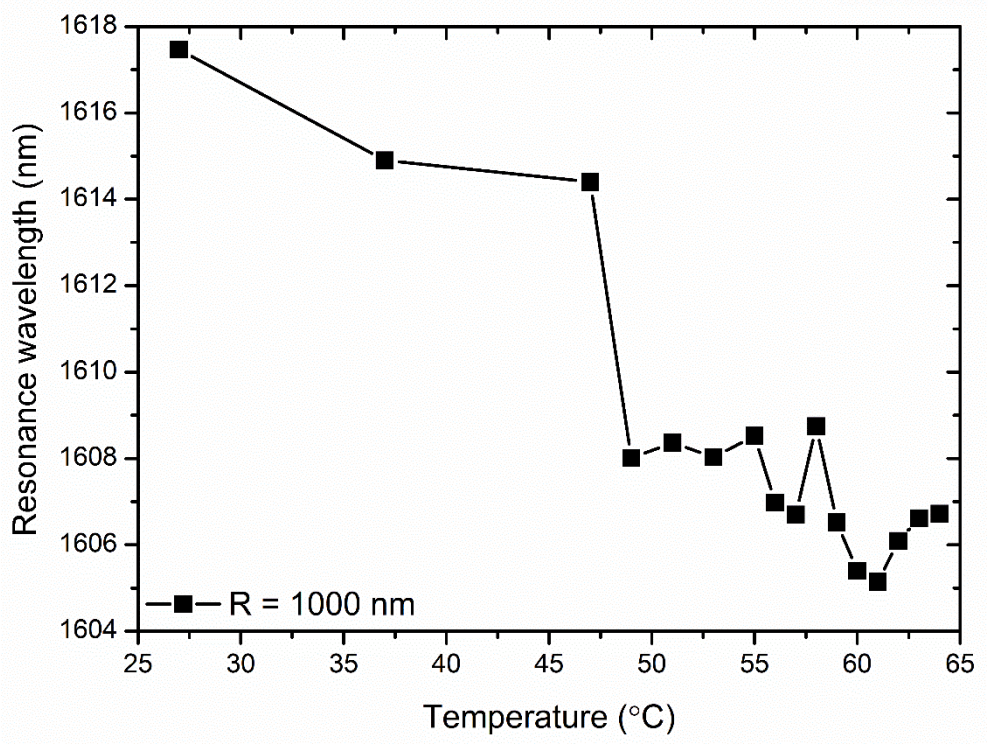

Figure 3-9: Temperature dependence of resonance wavelength in the experiment with LC E7 for the disk radius of 1000 nm

The range of the temperature at which the PDRs with LC were measured was from 27 °C to 64 °C. At the temperature higher than 47 °C, the PDRs were measured with more temperature points, to carefully observe any resonance wavelength transition nearby clearing temperature. The drop in the resonance wavelength (blue-shift) with respect to the temperature rise was observed, as expected, but there was only about 10-nm shift between the lowest temperature of 27 °C and the highest temperature of 64 °C.

4. Discussion

Although it is observed that the resonance wavelength drops with respect to temperature rise in both simulation and experiments, the wavelength shift in the experiment is shorter than the wavelength shift in the simulation, as shown in Figure 4-1, Figure 4-2 and Figure 4-3.

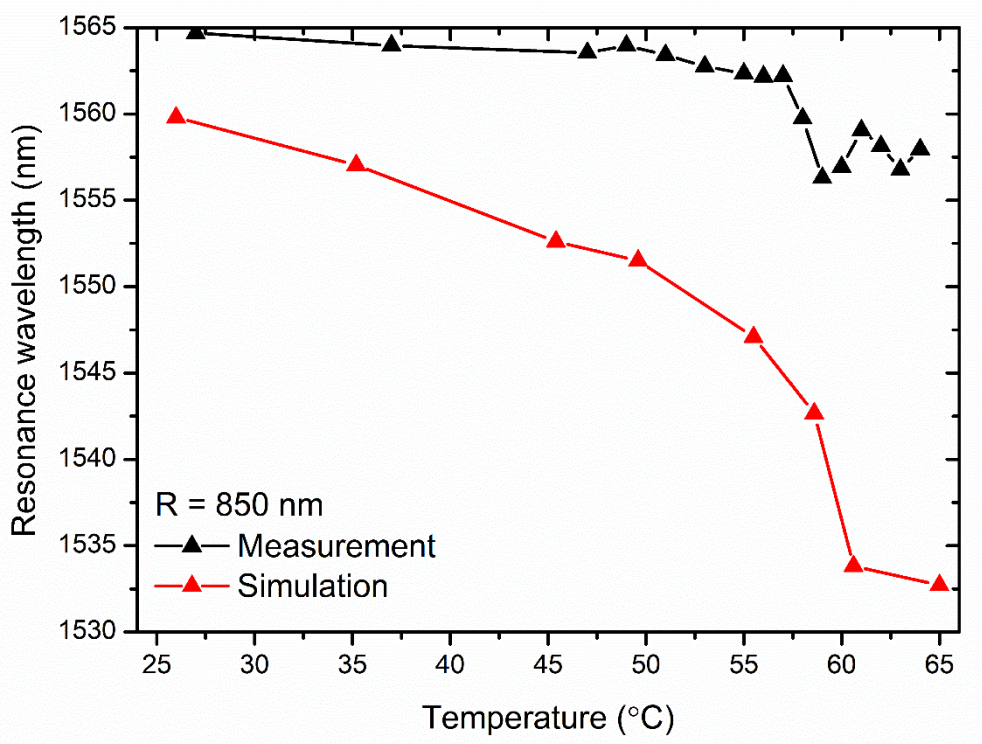

Figure 4-1: Comparison of the resonance wavelength shift with respect to rising temperature between simulation result and experimental result for the radius of 850 nm

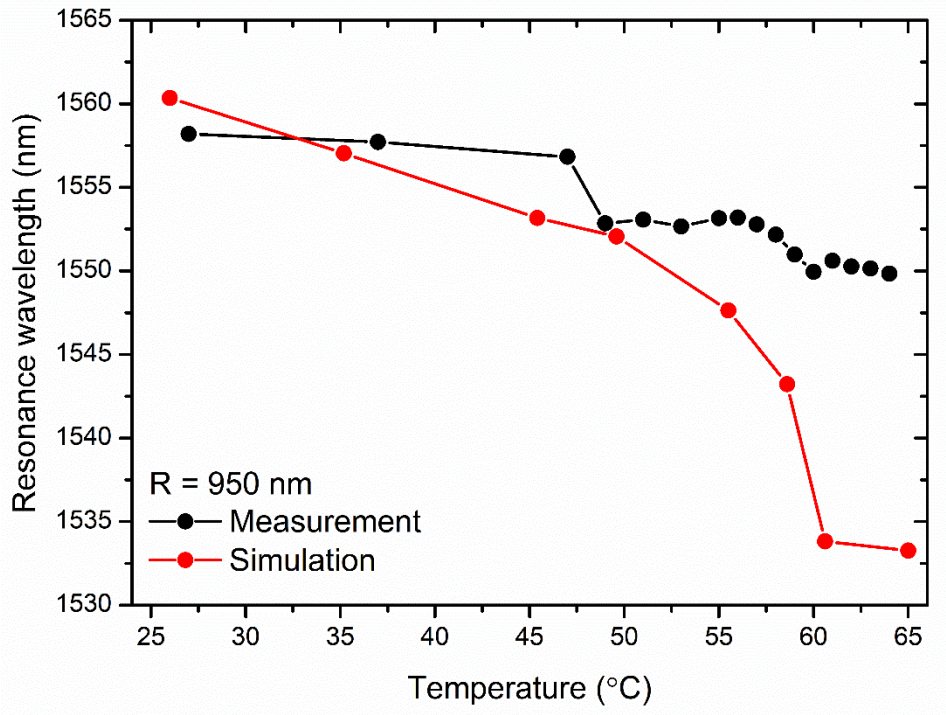

Figure 4-2: Comparison of the resonance wavelength shift with respect to rising temperature between simulation result and experimental result for the radius of 950 nm

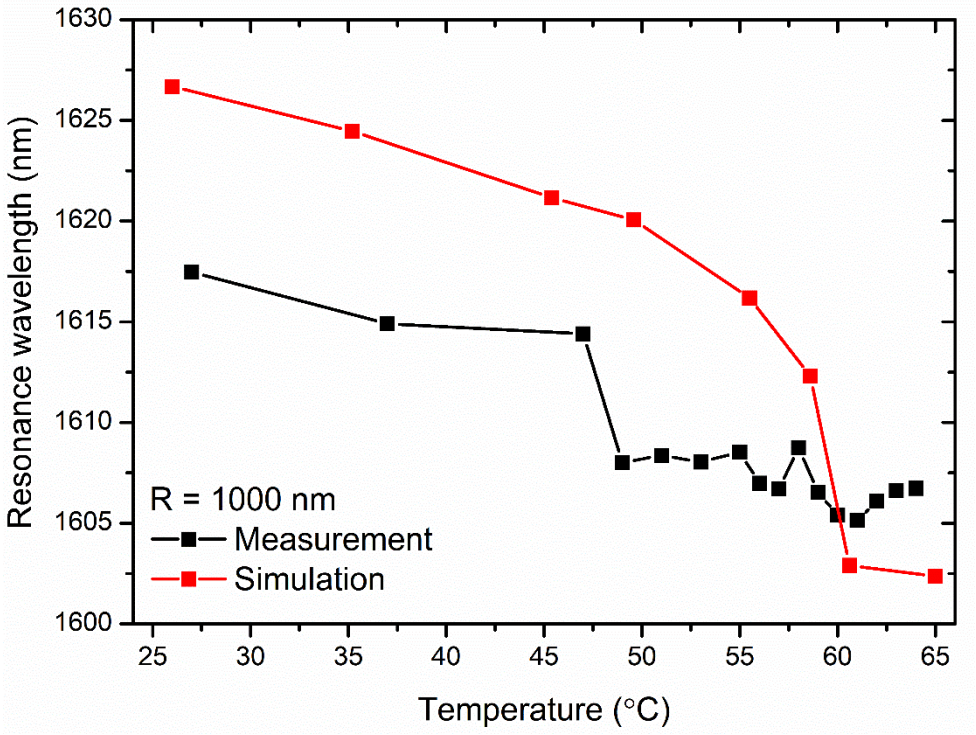

Figure 4-3: Comparison of the resonance wavelength shift with respect to rising temperature between simulation result and experimental result for the radius of 1000 nm

The short wavelength shift in the experimental results compared with simulation results may be attributed to a few reasons. First, the simulation was just a rough modelling and approximation of the LC-filled channel with the assumption that there would be two discrete regions with two different refractive indices. The positional and orientational order of the LC molecules in such a narrow channel, however, may be much more complicated. The second reason which may lead to the non-similar wavelength shift is the imperfect experiment condition. The time for measuring each reference waveguide or each PDR with the tunable laser source running from 1520 nm to 1630 nm takes about 2 minutes. During that time, the temperature fluctuates with the amplitude of ±0.4 °C due to the ambient temperature. Therefore, the measurement result might be affected somehow. Moreover, while conducting the experiments, I observed a phenomenon where there was a cloudy part inside the liquid crystal on the sample surface when the temperature was round 60 – 61 °C. This cloudy part did not account for the whole liquid crystal located on the sample, and could expand or shrink somehow randomly. On the screen for the zoom camera, there were somewhat “bubbles” inside the liquid and these bubbles disappeared when the temperature went beyond 62 °C. It is not ensured if the heat took effect with the LC molecules uniformly or just a part of the LC liquid poured onto the sample surface.

5. Conclusion

This thesis has introduced the experimental study of the Plasmofluidic Disk Resonators (PDRs) filled with liquid crystal. The work is to prove the resonance wavelength tuning ability of the PDRs when the characteristics of the liquid crystal change according to the temperature.

The PDRs filled with LC E7 under different temperatures were simulated and measured experimentally. Both simulation and experimental results agree that there is a blue-shift when the temperature rises, and the LC turning towards isotropic phase. The simulation results have shown the shift of about 30nm, whereas the experimental shift is just about 10nm. For some reasons, the experimental shift is modest compared with the simulation. Therefore, further effort needs to be done is optimizing the experiment condition.

This work is a step heading towards a higher-level massive work in the future which involves tuning the resonance wavelength of the PDRs filled with liquid crystal using electric field. To do so, the silicon disks need doping and there should be appropriately distributed metal electrodes deposited on the sample. The electric field controls the polarization of the liquid crystal molecules, which change the liquid crystal's characteristics. Electric field is expected to have more significant impact on liquid crystal molecule's positional and orientational order rather than temperature. Therefore, using liquid crystal for experiments of PDRs, there is a potential for developing a propitious electro-optical modulator.

REFERENCES

[1] W. Bogaerts, and L. Chrostowski, "Silicon Photonics Circuit Design: Methods, Tools and Challenges," *Laser & Photonics Reviews*, **12**, 1700237, 2018.

[2] G. T. Reed, *Silicon Photonics: The State of the Art*, John Wiley & Sons, Inc., 2008.

[3] L. Pavesi, and D. J. Lockwood, *Silicon Photonics*. Springer, 2004.

[4] W. Bogaerts, P. De Heyn, T. Van Vaerenbergh, K. De Vos, S. Kumar Selvaraja, T. Claes, P. Dumon, P. Bienstman, D. Van Thourhout, and R. Baets, "Silicon microring resonators", *Laser & Photonics Reviews*. **6**, 47-73, 2012.

[5] S. A. Maier, *Plasmonics: Fundamental and Applications*. Springer, 2007.

[6] M.-S. Kwon, "Metal-insulator-silicon-insulator-metal waveguides compatible with standard CMOS technology," *Optics Express*, **19**, 8379-8393, 2011.

[7] W. Sacher, T. Barwicz, B. J. F. Taylor, and J. Poon, "Polarization rotator-splitters in standard active silicon photonics platforms," *Optics Express*, **22**, 3777-3786, 2014.

[8] C. Li, and D. Dai, "Compact polarization beam splitter for silicon photonic integrated circuits with a 340-nm thick silicon core layer," *Optics Letters*, **42**, 4243-4246, 2017.

[9] J. Flueckiger, S. Schmidt, V. Donzella, A. Sherwali, D. M. Ratner, L. Chrostowski, and K. C. Cheung, "Sub-wavelength grating for enhanced ring resonator biosensor," *Optics. Express*, **24**, 15672-15686, 2016.

[10] Y. Zhang, Y. He, X. Jiang, B. Liu, C. Qiu, Y. Su, and R. A. Soref, "Ultra-compact and highly efficient silicon polarization splitter and rotator", *APL Photonics*, **1**, 091304, 2016.

[11] Y. Xu, and J. Xiao, "Ultracompact and high efficient silicon-based polarization splitter-rotator

using a partially-etched subwavelength grating coupler," *Scientific Reports*, **6**, 27949, 2016.

[12] Y. Ma, Y. Zhang, S. Yang, A. Novack, R. Ding, A. E. J. Lim, G. Q. Lo, B. J. Tom, and M. Hochberg, "Ultralow loss single layer submicron silicon waveguide crossing for SOI optical interconnect," *Optics Express*, **21**, 29374-29382, 2013.

[13] Z. Lu, H. Yun, Y. Wang, Z. Chen, F. Zhang, N. A. F. Jaeger, and Lukas Chrostowski, "Broadband silicon photonic directional coupler using asymmetric-waveguide based phase control," *Optics Express*, **23**, 3795-3808, 2015.

[14] M. Liu, X. Yin, E. U-A, B. Geng, T. Zentgraf, L. Ju, F. Wang, and Xiang Zhang, "A graphene-based broadband optical modulator," *Nature*, **474**, 64-67, 2011.

[15] R. Going, T. J. Seok, J. Loo, K. Hsu, and M. C. Wu, "Germanium wrap-around photodetectors on silicon photonics," *Optics Express*, **23**, 11975-11984, 2015.

[16] M. Wu, Z. Han, and V. Van, "Conductor-gap-silicon plasmonic waveguides and passive components at subwavelength scale," *Optics Express*, **18**, 11728-11736, 2010.

[17] M.-S. Kwon, B. Ku, and Y. Kim, "Plasmofluidic disk resonators," *Scientific Reports*, **6**, 23149, 2016.

[18] D. K. Yang, and S. T. Wu, *Fundamentals of Liquid Crystal Devices (2nd edition)*. Wiley & Sons, Inc., 2014.

[19] S. Brugioni and R. Meucci, "Refractive indices of liquid crystal E7 and K15 in the mid-and-near-IR regions," *Journal of Optical Technology*, 73, 315-317, 2006.

[20] J. Li, "Refractive Indices of Liquid Crystals and Their Applications in Display And Photonic Devices" *Ph. D Dissertation in* University of Central Florida, US, 2005.

[21] P. N. Sanda, D. B. Dove, and H. L. Ong, "Role of surface bonding on liquid-crystal alignment at metal surface," *Physical Review A*, **39**, 2653-2658, 1989.

[22] Y. Garbovskiy, L. Reisman, Z. Celinski, R. E. Camley, and A. Glushchenko, "Metallic surfaces as alignment layers for nondisplay applications of liquid crystals," *Applied Physics Letters,* **98**, 073301, 2011.

[23] A. Pizzirusso, R. Berardi, L. Muccioli, M. Ricci, and C. Zannoni, "Predicting surface anchoring: molecular organization across a thin film of 5CB liquid crystal on silicon," *Chemical Science,* **3**, 573-579, 2012.

[24] F. Ercole, T. P. Davis, and Richard A. Evans, "Photo-responsive systems and biomaterials: photochromic polymers, light-triggered self-assembly, surface modification, fluorescence modulation and beyond," *Polymer Chemistry*, **1**, 37-54, 2010.

[25] S. Zhan, X. Wang, and Y. Liu, "Fast centroid algorithm for determining the surface plasmon resonance angle using the fixed-boundary method", *Measurement Science and Technology*, **19**, 025201, 2017.